Supporting Information: Time-Dependent Screening Explains the Ultrafast Excitonic Signal Rise in 2D Semiconductors

Valerie Smejkal,[*,†] Florian Libisch,[*,†] Alejandro Molina-Sanchez,[‡] Chiara Trovatello,[¶] Ludger Wirtz,[§] and Andrea Marini[‖]

†*Vienna University of Technology, Institute for Theoretical Physics, 1040 Vienna, Austria, EU*

‡*Institute of Materials Science (ICMUV), University of Valencia, Valencia, Spain, EU*

¶*Department of Physics, Politecnico di Milano, P. Leonardo da Vinci 32, 20133 Milan, Italy, EU*

§*Department of Physics and Materials Science, University of Luxembourg, 1511 Luxembourg, Luxembourg, EU*

‖*CNR-ISM, Division of Ultrafast Processes in Materials (FLASHit), Area della Ricerca di Roma 1, Via Salaria Km 29.3, I-00016 Monterotondo Scalo, Italy, EU*

E-mail: valerie.smejkal@tuwien.ac.at; florian.libisch@tuwien.ac.at

Theoretical details and simulation workflow

Ground state properties. In our theoretical description, we first calculate the ground state properties of a free-standing MoS_2 monolayer using density functional theory (DFT) as

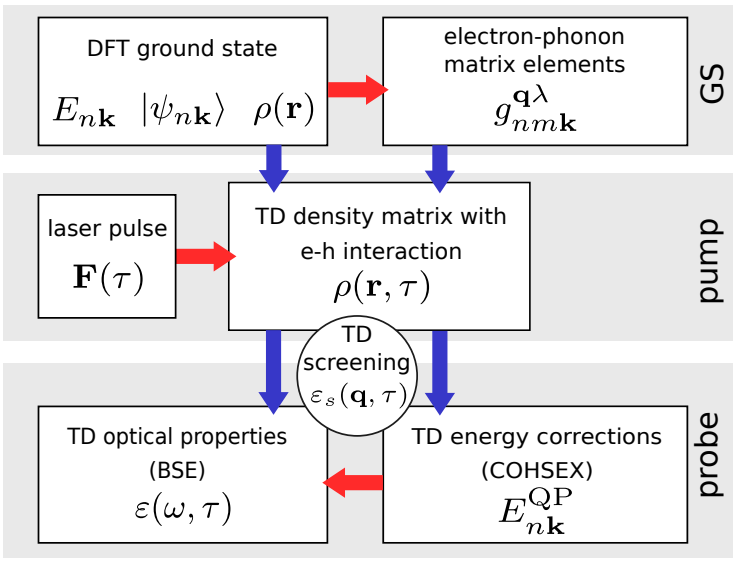

Figure S1: Workflow of the simulations.

implemented in the `pwscf`-code[S1,S2] (Quantum Espresso package). We use fully relativistic pseudopotentials taking into account the spin-orbit coupling that leads to the spin-split A- and B-exciton. The electron-phonon matrix elements are obtained using density functional perturbation theory (DFPT).

Pump-pulse interaction. Starting from the DFT ground state, we solve the equation of motion for the time-diagonal lesser Green's function, *i.e.,* the density matrix $\rho_l(\tau)$, in an external electric field $\mathbf{F}(\tau)$. By incorporating the variation of the self-energy $\Delta\Sigma^{\mathrm{H_{xc}}}$, we can correctly describe the electron-hole interaction which the photoexcited carriers experience. This part describes the coherent dynamics of the system $\frac{\partial\rho_l(\tau)}{\partial\tau}|_{\mathrm{coh}}$ and, in the limit of linear response, is equivalent to the Bethe-Salpeter equation (BSE),[S3] which has been used very successfully to describe the optical spectra in monolayer TMDs. The equation of motion reads

$$\frac{\partial\rho_l(\tau)}{\partial\tau} = \underbrace{\Delta\tilde{\epsilon}_l\rho_l(\tau) + [U^{\mathrm{pump}}(\tau),\rho]_l + \left[\Delta\Sigma^{\mathrm{H_{xc}}}(\tau),\rho\right]_l}_{\frac{\partial\rho_l(\tau)}{\partial\tau}|_{\mathrm{coh}}} + \frac{\partial\rho_l(\tau)}{\partial\tau}|_{\mathrm{coll}} \quad . \tag{1}$$

Here, $l = \{nm\mathbf{k}\}$ is a generalized index of the band and $\mathbf{k}$-point where $\{n,m\}$ run through all bands included in the real-time simulation, $\Delta\tilde{\epsilon}_l = \epsilon^{KS}_{n\mathbf{k}} - \epsilon^{KS}_{m\mathbf{k}} + \Delta^{\mathrm{scissor}}$ is the difference

between quasi-particle energies where we add a scissor operator $\Delta^{\text{scissor}} = 0.991$ eV making up for the underestimation of the band gap in DFT and $U^{\text{pump}} = -\hat{\mathbf{r}} \cdot \mathbf{F}(\tau)$ is the interaction with the external field.

$\frac{\partial \rho_l(\tau)}{\partial \tau}|_{\text{coll}}$[S4,S5] is the collisions term in the equations of motion. It contains the scattering mechanisms. Here, we take into account first-principles electron-phonon scattering which causes the excited state population to thermalize. For the relaxation to the ground state, we use a phenomenological decay time $T_{\text{decay}} = 670\,\text{fs}$ which causes the excited population to decay exponentially. We extract this time by fitting an exponential to the experimental data between 100 fs-200 fs [see Fig. S4], *i.e.*, after the pulse and the associated signal buildup are already over. Consequently, it is not a free parameter and it is not fitted to reproduce any specific feature of the short-time buildup. Similar decay times have previously been attributed to defect scattering.[S6]

Simulation of the probe. The probe spectra are simulated based on the time-dependent carriers $\rho_{nn\mathbf{k}}(\tau) = f_{n\mathbf{k}}(\tau)$ obtained from the solution of Eq. (1). First we obtain the excitation- and time-dependent static screening $\varepsilon_s(\mathbf{q}, \tau)$ of the material.[S7] The screening is calculated within the random phase approximation (RPA)

$$\varepsilon^{-1}_{\mathbf{GG'}}(\mathbf{q};\tau) = \delta_{\mathbf{GG'}} + V^t_{\mathbf{GG'}}(\mathbf{q})\chi^{RPA}_{\mathbf{GG'}}(\mathbf{q};\tau) \quad , \tag{2}$$

where $V^t(\mathbf{q})$ is the truncated Coulomb interaction introduced to avoid spurious interactions between periodic images from the supercell calculation.[S8] $\chi^{RPA}(\mathbf{q};\tau)$ is the RPA polarization function we get from solving the Dyson equation

$$\chi^{RPA}_{\mathbf{GG'}}(\mathbf{q};\tau) = \chi^0_{\mathbf{GG'}}(\mathbf{q};\tau) + \sum_{\mathbf{G}_1\mathbf{G}_2} \chi^0_{\mathbf{GG}_1}(\mathbf{q};\tau)V^t_{\mathbf{G}_1\mathbf{G}_2}(\mathbf{q})\delta_{\mathbf{G}_1,\mathbf{G}_2}\chi^{RPA}_{\mathbf{G}_2\mathbf{G'}}(\mathbf{q};\tau) \quad . \tag{3}$$

The time-dependent occupations enter the calculation of the independent particle polariza-

tion function $\chi^0_{\mathbf{G}\mathbf{G}'}(\mathbf{q},;\tau)$

$$\chi^0_{\mathbf{G}\mathbf{G}'}(\mathbf{q};\tau) \overset{\omega\to 0}{=} 2\sum_{n,m}\int_{BZ}\frac{d\mathbf{k}}{(2\pi)^3} D^*_{nm}(\mathbf{k},\mathbf{q},\mathbf{G}) D_{nm}(\mathbf{k},\mathbf{q},\mathbf{G}') f_{n\mathbf{k}-\mathbf{q}}(\tau)(1-f_{m\mathbf{k}}(\tau))\times \\ \times\left[\frac{1}{\omega+\epsilon_{m\mathbf{k}-\mathbf{q}}-\epsilon_{n\mathbf{k}}+i0^+}-\frac{1}{\omega+\epsilon_{n\mathbf{k}}-\epsilon_{m\mathbf{k}-\mathbf{q}}-i0^+}\right] \quad , \tag{4}$$

where n, m run over all bands and $D_{nm}(\mathbf{k},\mathbf{q},\mathbf{G}) = \langle n\mathbf{k}|\, e^{i(\mathbf{q}+\mathbf{G})\cdot\mathbf{r}}\, |m\mathbf{k}-\mathbf{q}\rangle$ are the screening matrix elements. Note that $D_{eh}(\mathbf{k},\mathbf{q})$ in the main text is $D_{n=e,m=h}(\mathbf{k},\mathbf{q},\mathbf{G}=0)$. This altered screening together with the direct influence of the excited carriers is used to obtain the change of the electronic energy levels in the Coulomb hole plus screened exchange (COHSEX) approximation. Then, the optical properties of the material are calculated using the BSE with a now time-dependent kernel, see Eq. (2) in the Methods section of the main text. This description contains the BGR, the reduction of the EBR as well as Pauli blocking by excited carriers. The workflow of the simulations is depicted in Fig. S1.

Convergence parameters

Ground state and phonon modes. We use norm-conserving, fully relativistic pseudopotentials for Mo and S. Only the symmorphic subset of the symmetries is employed by setting force_symmorphic=.true. The monolayer is simulated using a supercell approach with a layer spacing of 25 Bohr in the out-of-plane direction. The ground state is converged on an $18 \times 18 \times 1$ grid with a plane wave cutoff of 120 Ry. The nine phonon modes of monolayer MoS_2 are calculated on a non-self-consistent $30 \times 30 \times 1$ **k**-grid.

Real-time calculations. The real-time simulations are performed on the same $30\times30\times1$ **k**-grid where the phonon modes have been calculated. For better convergence, we resort to a double-grid technique on a $61\times61\times1$ grid.[S9] We propagate two valence and eight conduction bands of MoS_2 where a scissor operator of 0.991 eV is introduced to shift the absorption onset of the A-exciton to 1.90 eV. To avoid spurious interactions between periodic images

of the monolayer, we employ a Coulomb interaction truncation of 23 Bohr (integration of the relevant integrals is done on a random **q**-grid of 1000000 points).[S8,S10] The time step for the time evolution of the density matrix is $\Delta t = 10\,\text{as}$ and the scattering time step is $\Delta t_{\text{scatt}} = 1\,\text{fs}$. The decay time of the excited population is set to $T_{\text{decay}} = 670\,\text{fs}$ and the off-diagonal matrix elements are dephased with a state-dependent dephasing rate of $\Gamma_{n\mathbf{k}} = [0.02 + 0.03 \cdot (E_{n\mathbf{k}} - E_{\text{ref}})]\,\text{eV}$ where E_{ref} is set to the edge onset of the conduction (valence) band for electrons (holes). The interaction potentials are represented in Fourier space with a cutoff for the transition matrix elements (30 Ry), the Hartree potential (15 Ry), the exchange (25 Ry) and the correlation (3500 mRy). We use 70 bands for the screening matrix which is cut off at 3500 mRy. The parameters for the real time simulations were carefully converged w.r.t. change of the excited carrier density.

Probe-pulse: energy renormalization and optical properties. The carrier-induced changes to the probe spectrum are calculated on the real-time $30 \times 30 \times 1$ **k**-grid for two valence and two conduction bands. We employ the same Coulomb interaction truncation already used in the time-evolution. We use 70 bands for the screening matrix which is cut off at 4000 mRy and a cutoff for the transition matrix elements of 40 Ry. The reciprocal lattice vectors used for the exchange energy in the COHSEX calculation are cut off at 40 Ry. In the calculation of the Bethe-Salpeter equation we use the same scissor operator of 0.991 eV as in the real-time simulations and an energy-dependent broadening of $\Gamma(\omega) = [0.039 + 0.095 \cdot (\omega - 1.7)]\,\text{eV}$ which was fit to the width of the experimental absorption spectrum.

Extended data

Carrier dynamics

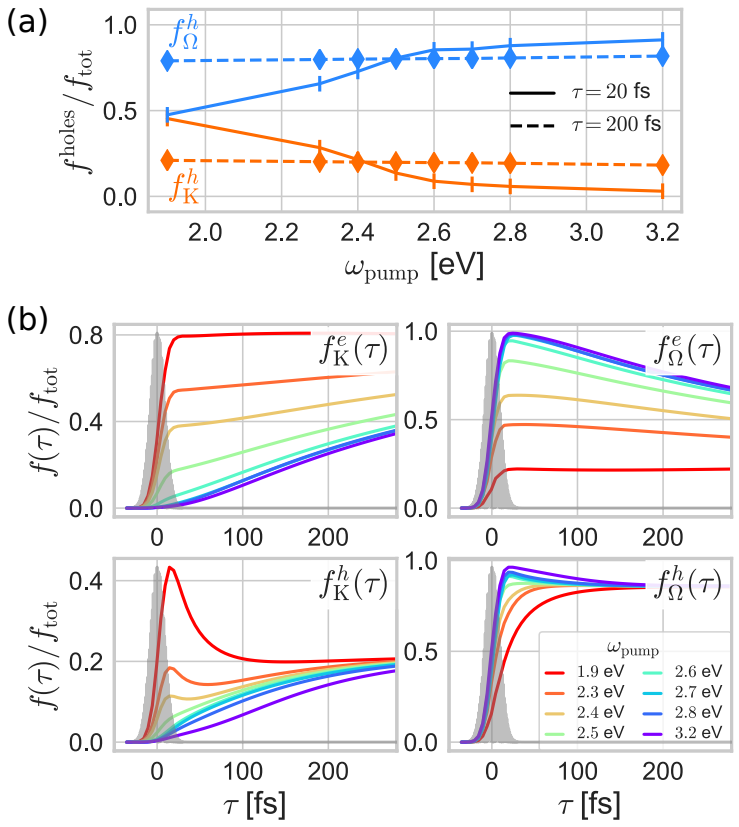

Figure S2: (a) Pump-energy-dependent contribution of f_{K} and of f_Ω to the total number of excited holes right after the pump (solid line) and at a 200 fs delay time (dashed line). Already during the pump, there is a fast redistribution of excited holes from the *Active Excitonic Regions* to states around the Γ-point which is energetically close and has a larger density of states. Already at 200 fs, there is a quasi–equilibrium between Γ and K. (b) Time–dependent dynamics of electrons e and holes h for f_{K} and of f_Ω.

Transient reflection and $\Delta\varepsilon$

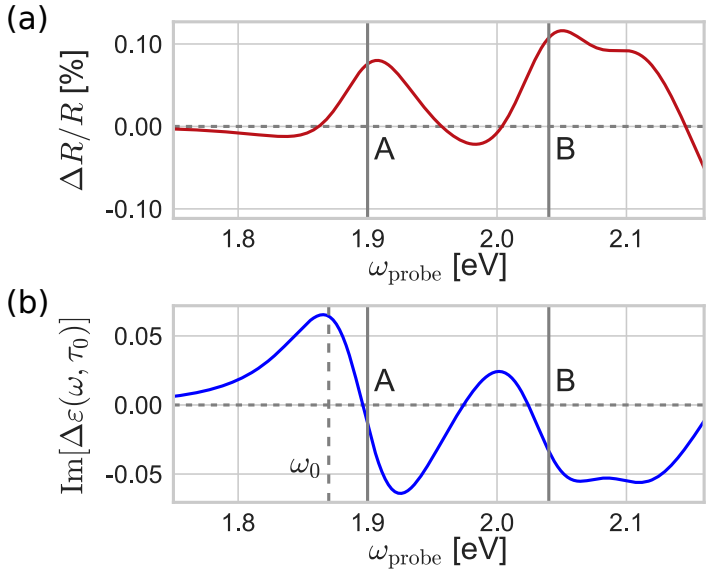

Figure S3: (a) Transient reflection spectrum from the SiO_2/Si stack at $\tau_0 = 200\,\mathrm{fs}$ for a pump with $\omega_{\mathrm{pump}} = 2.80\,\mathrm{eV}$. (b) Probe-energy-dependent change of the optical absorption $\Delta A(\omega, \tau_0) \propto \Delta\mathrm{Im}\left[\varepsilon(\omega, \tau_0)\right]$ at $\tau_0 = 200\,\mathrm{fs}$ for a pump with $\omega_{\mathrm{pump}} = 2.80\,\mathrm{eV}$. The solid vertical lines denote the position of the A- and B-exciton. ω_0 is the constant energy used for Fig. 5 in the main text.

Decay time

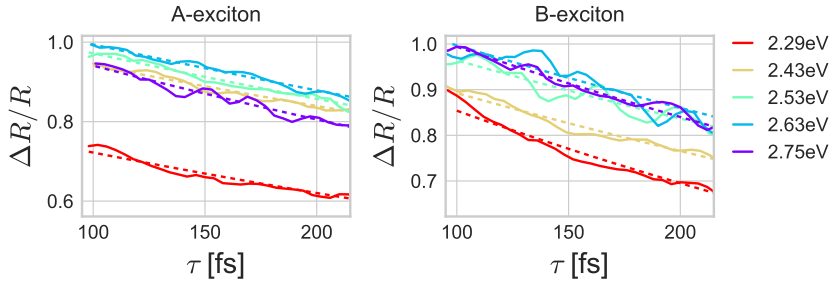

Figure S4: Experimental transient reflectivity data between 100 fs–200 fs together with the exponential fit. The average decay time of the signal at the A-exciton is $\overline{T}^{\mathrm{A}}_{\mathrm{decay}} = 724\,\mathrm{fs}$ and at the B-exciton is $\overline{T}^{\mathrm{B}}_{\mathrm{decay}} = 610\,\mathrm{fs}$.

Transient reflection without decay

When we neglect the decay of the excited population, we see a clear two-stage behavior of the time–dependent constant energy cuts through the transient reflection, see Fig. S5.

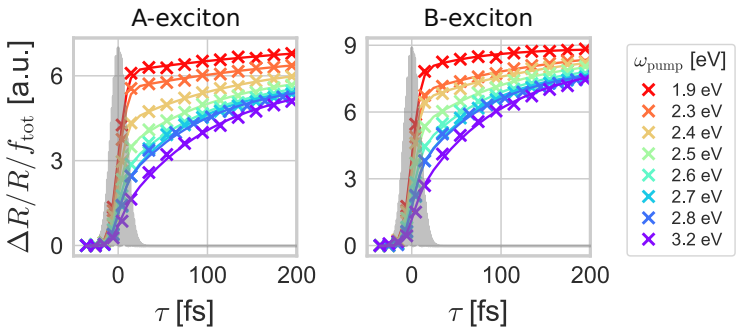

Figure S5: Time–dependent constant energy cuts of the transient reflection at the A- and B- excitonic resonance without decay. The markers are the simulated data points while the solid lines give the fit. Different pump energies are normalized to the total number of excited carriers $f_{\mathrm{tot}}(\omega_{\mathrm{pump}})$ which varies due to the energy–dependent optical absorption cross section.

This behavior can be modeled in terms of occupation residing in the *Active Excitonic Regions* $f_{\mathrm{K}}(\tau)$ and in the rest of the BZ $f_{\Omega}(\tau)$. The total excited population $f_{\mathrm{tot}}(\tau)$ is given by the sum of the two

$$f_{\mathrm{tot}}(\tau) = f_{\Omega}(\tau) + f_{\mathrm{K}}(\tau) \quad . \tag{5}$$

Its dynamics follows the intensity of the pulse $I(\tau) = e^{-\tau^2/\sigma^2}$.

$$\frac{\partial f_{\mathrm{tot}}(\tau)}{\partial \tau} = f_0 \times \frac{I(\tau)}{\sqrt{\pi\sigma^2}} \quad , \tag{6}$$

where f_0 is the maximum occupation, with the solution

$$f_{\mathrm{tot}}(\tau) = \frac{f_0}{2}\left[1 - erf\left(\frac{-\tau}{\sigma}\right)\right] \quad . \tag{7}$$

The excitation by the pump pulse is followed by an excitation-conserving dynamics from $f_{\Omega}(\tau)$ to the minimum of the excited system f_{K} with a mean time constant $T_{\mathrm{el-ph}}$.

$$\frac{\partial f_\Omega(\tau)}{\partial \tau} = \underbrace{(1-\nu)\frac{\partial f_{\rm tot}(\tau)}{\partial \tau}}_{\rm resonant} - \underbrace{\frac{f_\Omega(\tau)}{T_{\rm el-ph}}}_{\rm relaxation} \quad . \tag{8}$$

Here, $(1-\nu)$ is the fraction of the occupation which is resonantly excited into f_Ω.

We can obtain the occupation at the *Active Excitonic Regions* by substituting into the conservation of excited carriers

$$f_{\rm K}(\tau) = f_{\rm tot}(\tau) - f_\Omega(\tau) \quad . \tag{9}$$

This model for $f_{\rm K}$ fits the time-dependent transient reflection curves, Fig. S5, very well.

References

(S1) Giannozzi, P.; Andreussi, O.; Brumme, T.; Bunau, O.; Buongiorno Nardelli, M.; Calandra, M.; Car, R.; Cavazzoni, C.; Ceresoli, D.; Cococcioni, M.; Colonna, N.; Carnimeo, I.; Dal Corso, A.; de Gironcoli, S.; Delugas, P.; DiStasio, R. A.; Ferretti, A.; Floris, A.; Fratesi, G.; Fugallo, G. *et al.* Advanced Capabilities for Materials Modelling with Quantum ESPRESSO. *Journal of Physics: Condensed Matter* **2017**, *29*, 465901.

(S2) Giannozzi, P.; Baseggio, O.; Bonfà, P.; Brunato, D.; Car, R.; Carnimeo, I.; Cavazzoni, C.; De Gironcoli, S.; Delugas, P.; Ferrari Ruffino, F.; Ferretti, A.; Marzari, N.; Timrov, I.; Urru, A.; Baroni, S. Quantum ESPRESSO Toward the Exascale. *Journal of Chemical Physics* **2020**, *152*, 154105.

(S3) Attaccalite, C.; Grüning, M.; Marini, A. Real-Time Approach to the Optical Properties of Solids and Nanostructures: Time-Dependent Bethe-Salpeter Equation. *Physical Review B* **2011**, *84*, 245110.

(S4) Marini, A. Competition Between the Electronic and Phonon-Mediated Scattering Channels in the Out-of-Equilibrium Carrier Dynamics of Semiconductors: An *ab Initio* Approach. *Journal of Physics: Conference Series* **2013**, *427*.

(S5) Sangalli, D.; Marini, A. Complete Collisions Approximation to the Kadanoff-Baym Equation: A First-Principles Implementation. *Journal of Physics: Conference Series* **2015**, *609*.

(S6) Cunningham, P. D.; McCreary, K. M.; Hanbicki, A. T.; Currie, M.; Jonker, B. T.; Hayden, L. M. Charge Trapping and Exciton Dynamics in Large-Area CVD Grown MoS_2. *Journal of Physical Chemistry C* **2016**, *120*, 5819–5826.

(S7) Sangalli, D.; Dal Conte, S.; Manzoni, C.; Cerullo, G.; Marini, A. Nonequilibrium

Optical Properties in Semiconductors from First Principles: A Combined Theoretical and Experimental Study of Bulk Silicon. *Physical Review B* **2016**, *93*, 195205.

(S8) Rozzi, C. A.; Varsano, D.; Marini, A.; Gross, E. K.; Rubio, A. Exact Coulomb Cutoff Technique for Supercell Calculations. *Physical Review B* **2006**, *73*, 205119.

(S9) Sangalli, D.; Ferretti, A.; Miranda, H.; Attaccalite, C.; Marri, I.; Cannuccia, E.; Melo, P.; Marsili, M.; Paleari, F.; Marrazzo, A.; Prandini, G.; Bonfà, P.; Atambo, M. O.; Affinito, F.; Palummo, M.; Molina-Sánchez, A.; Hogan, C.; Grüning, M.; Varsano, D.; Marini, A. Many-Body Perturbation Theory Calculations Using the Yambo Code. *Journal of Physics: Condensed Matter* **2019**, *31*, 32.

(S10) Marini, A.; Hogan, C.; Grüning, M.; Varsano, D. Yambo: An *ab Initio* Tool for Excited State Calculations. *Computer Physics Communications* **2009**, *180*, 1392–1403.